

**Local spectroscopy of a Kondo impurity: Co on Au(111)**

V. Madhavan, W. Chen,\* T. Jamneala, and M. F. Crommie

*Department of Physics, University of California at Berkeley, Berkeley, California 94720-7300  
and Materials Sciences Division, Lawrence Berkeley Laboratory, Berkeley, California 94720-7300*

Ned S. Wingreen

*NEC Research Institute, 4 Independence Way, Princeton, New Jersey 08540*

(Received 26 March 2001; published 8 October 2001)

We present a detailed study of the local electronic properties of the Kondo system formed from cobalt adatoms deposited onto Au(111) at a temperature of 6.6 K. Cryogenic scanning-tunneling spectroscopy was used to observe impurity-induced resonances at the Fermi energy and at the Au(111) surface-state band edge. The line shape of the Fermi-energy resonance, identified as a Kondo resonance, is observed to vary with lateral position from the impurity center and with impurity binding position on the reconstructed Au(111) surface. Little vertical dependence is seen in the resonance line shape for positions above the center of the impurity. Interaction effects between Kondo impurities are observed to remain small as cobalt coverage is increased up to 1 ML on the gold surface. The Kondo resonance is shown theoretically to be a member of a general class of Fano resonances arising from the interaction of a discrete impurity state with a conduction-electron continuum. The asymmetric line shape of the resonance thus reflects quantum interference between the  $d$  orbital and continuum conduction electron channels, as well as their coupling to the STM tip.

DOI: 10.1103/PhysRevB.64.165412

PACS number(s): 72.10.Fk, 72.15.Qm, 73.20.Hb, 73.20.At

**I. INTRODUCTION**

The coupling between spin and electronic degrees of freedom in condensed-matter systems leads to a variety of phenomena, some of which have useful technological applications. Examples are giant and colossal magnetoresistance,<sup>1,2</sup> spin-polarized tunneling,<sup>3,4</sup> and the Kondo effect.<sup>5</sup> The Kondo effect occurs in magnetic structures at the atomic scale, and typically arises from spin-flip scattering between a single magnetic atom and the electrons of a metal host. This interaction causes a correlated screening cloud to form around the impurity atom, leading to anomalous behavior in the resistivity, specific heat, and magnetic susceptibility of dilute magnetic alloys.<sup>5,6</sup> While most measurements of Kondo alloys have involved macroscopic averages, Kondo impurities are extremely local perturbations to a solid. Few experimental studies have been performed that directly probe the local properties of these strongly interacting impurities. This paper focuses on a scanning-tunneling-microscopy (STM) study of individual cobalt adatoms and is aimed at forming a better understanding of the local electronic properties of Kondo impurities.

Tunneling experiments have been used extensively to study the density of states (DOS) of Kondo systems, particularly the formation of the Kondo resonance at temperatures below the Kondo temperature  $T_K$ . Most of these studies have involved macroscopic metal-insulator-metal junctions doped with magnetic atoms,<sup>7</sup> although crossed-wire experiments<sup>8</sup> and “nanobridge” techniques have also been used.<sup>9</sup> Recently, STM has been used to probe well-characterized, individual Kondo impurities at surfaces.<sup>10–13</sup> The first STM studies of magnetic atoms involved systems with very low Kondo temperatures, such as Fe adatoms on Pt,<sup>14</sup> W,<sup>15</sup> and Nb (Ref. 16) surfaces. These experiments showed signs of magnetic  $d$  states and Cooper-pair destruc-

tion (for superconducting substrates), but no signs of the Kondo resonance, ostensibly because the experimental temperature was greater than  $T_K$ . Cryogenic STM experiments performed on impurity systems with higher Kondo temperatures (such as Co adatoms on Au<sup>10</sup> and Cu<sup>12</sup> surfaces, as well as Ce adatoms on Ag<sup>11</sup>) have recently been successful in observing the Kondo resonance for individual magnetic atoms. Interactions between Kondo impurities have also been studied recently using atomic manipulation.<sup>17</sup>

Here we discuss a study of the Kondo system formed from individual cobalt atoms deposited onto a Au(111) substrate at a temperature of 6 K. Some results have been published on this system already,<sup>10</sup> but here we provide a more in-depth presentation of experimental results and of our theoretical understanding of the impurity behavior. In summary, we have performed local spectroscopic measurements to investigate the electronic structure of this surface Kondo system over the energy range  $\pm 1$  eV around  $E_F$ . We find resonances in the electronic structure at “high energy” ( $-0.4$  eV from  $E_F$ ) and at “low energy” ( $0.010$  eV from  $E_F$ ) for individual cobalt atoms. We believe these resonances arise from a combination of an impurity-induced defect state and the Kondo resonance. The line shape of the Kondo resonance was observed to depend on the lateral position of the STM tip with respect to an impurity atom’s center, but the line shape was not observed to vary significantly with the vertical position of the tip. The Au(111) surface reconstruction was observed to have a pronounced effect on Kondo impurity behavior, as seen by positioning cobalt atoms in different regions of the reconstruction unit cell. Interaction between cobalt impurity atoms was studied by obtaining STM spectra at different cobalt surface coverages. Some disappearance of the Kondo resonance was observed, which we attribute to cobalt-cobalt clustering, but the line shape and magnitude remained essentially unchanged for those atoms displaying

the Kondo resonance. This implies that long-range interactions between cobalt atoms are weak.

In order to better understand the experimentally observed impurity behavior, we have calculated the expected tunnel current into a single Kondo impurity from an STM tip. This calculation uses the Anderson model<sup>18</sup> and the transfer-Hamiltonian-tunneling formalism,<sup>19</sup> and reproduces the asymmetric line shape observed in our spectroscopic measurements. The Kondo resonance is seen to manifest itself as a type of Fano resonance<sup>20</sup> involving quantum interference between  $d$  orbitals and conduction-electron-tunneling channels. While several theoretical treatments are now published on this topic,<sup>10,11,21–24</sup> here we lay special emphasis on the similarity between the tunneling configuration and Fano's original treatment of resonance spectroscopy. Comparisons between impurity calculations and experimental results are used to help clarify the interaction between impurity  $d$ -orbital and conduction-electron degrees of freedom for Co atoms on gold.

In Sec. II we discuss (a) experimental details, (b) impurity spectra including STM tip-height dependence, (c) cobalt surface site and lateral spatial dependence of spectra, as well as the (d) coverage dependence of the spectra. In Sec. III we present (a) an overview of impurity electronic structure, (b) a discussion of noninteracting impurities and the Fano resonance, (c) a discussion of interacting impurities and the Kondo resonance, and a discussion of (d) impurity/tip coupling and (e) density-dependent interaction effects. Section IV contains a summary.

## II. EXPERIMENTAL RESULTS

### A. STM and substrate

The experiments described here were performed using a home-built cryogenic STM ( $T=6$  K) in ultrahigh vacuum. Clean gold surfaces were prepared by putting single-crystal Au(111) substrates through cycles of argon sputtering and annealing. Surfaces prepared in this way were transferred in UHV to the low-temperature STM. Cobalt adsorbate atoms (adatoms) were deposited onto the low-temperature surface through line-of-sight e-beam evaporation. STM tunneling spectra ( $dI/dV$ ) were measured by placing a 200–500 Hz ac modulation signal (with rms amplitude in the range of 1–10 mV) onto the tunnel bias voltage and then using lock-in detection of the resulting ac tunnel current.  $dI/dV$  spectra were obtained under open feedback loop conditions to keep the STM tip stable.

Gold provides a useful substrate for these studies because it is known to yield a high Kondo temperature for cobalt impurities in the bulk<sup>25–27</sup> ( $T_K$  between 300–700 K) and at a surface<sup>28</sup> ( $T_K \approx 19$  K). In order to observe the fully developed Kondo resonance, the experimental temperature (6 K) must be less than  $T_K$ . The Au(111) surface, however, is not a structureless metallic background. Au(111) displays a complex, long-range atomic reconstruction, as well as a delocalized two-dimensional electronic surface state. This reconstruction is known as the “herringbone” reconstruction and has a  $22 \times \sqrt{3}$  symmetry that divides the surface into hcp (hexagonal-close-packed) and fcc (face-centered-cubic) do-

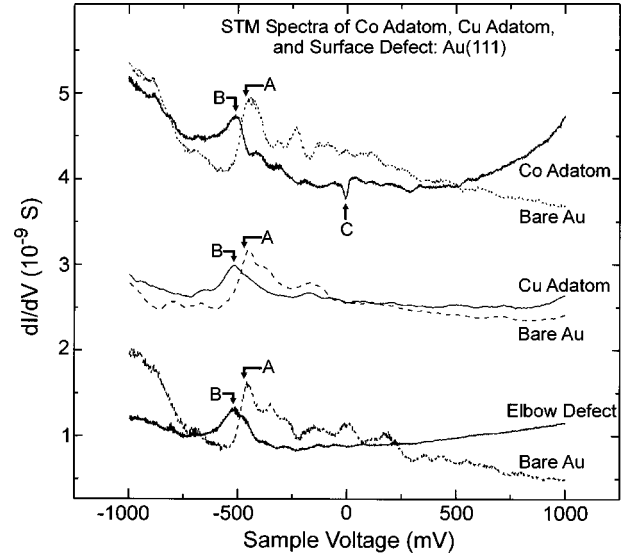


FIG. 1.  $dI/dV$  spectra obtained with the STM tip held over a single Co adatom on Au(111), a single Cu adatom on Au(111), and a single Au(111) point defect. A bare Au(111) spectrum measured with the same tip is shown in each case as a reference (each pair of spectra were measured with a different tip). “A” marks the surface-state band edge while “B” marks the location of the band-edge resonance induced in each case. Only the Co adatom induces formation of a narrow Kondo resonance at  $E_F$ , marked “C.” Cobalt-atom curves and elbow-defect curves have been vertically shifted by  $1.5 \times 10^{-9}$  and  $-1.7 \times 10^{-9}$  S, respectively.

mains separated by “soliton” walls.<sup>29</sup> The Shockley surface state that coexists with this reconstruction provides a background two-dimensional electron band that crosses  $E_F$ .<sup>30</sup>

### B. Impurity spectra and vertical dependence

Figure 1 shows a  $dI/dV$  spectrum measured while holding the STM tip over a single cobalt atom on Au(111), as well as a spectrum measured with the same tip over an adjacent bare gold region (the center of the cobalt atom is located at least 15 Å from the center of a herringbone domain wall). As experimental controls, spectra are also shown that were measured with the tip held on and off a single adsorbed copper atom on Au(111) and on a point-defect at the “elbow” of the Au reconstruction. The spectra measured over bare gold correspond to a convolution of the electronic structure of the Au(111) surface and the STM tip over the energy range  $\pm 1$  eV around  $E_F$ .<sup>31</sup> Small features in the bare-gold spectra arise from a combination of tip-electronic structure and surface-electronic structure due to quantum interference of two-dimensional surface-state electrons scattering from random surface structures. The dominant feature in the bare Au spectra is the sharp dropoff (for descending voltages) labeled “A.” This point marks the Au(111) surface-state band edge and lies at an energy 460 mV below  $E_F$  (as measured from the start of the downward transition). The influence of the herringbone reconstruction on this spectrum has been studied previously.<sup>32,33</sup>

When the STM tip is placed over a cobalt atom, the  $dI/dV$  spectrum changes markedly. The structure seen in the

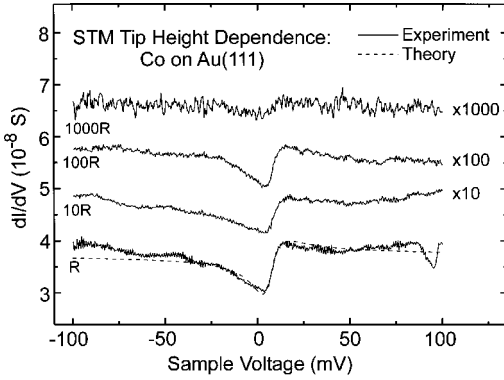


FIG. 2. Solid lines show  $dI/dV$  spectra measured with the STM tip held at different heights above a single Co atom on Au(111). Bottom curve corresponds to junction resistance  $R=2\times 10^8\ \Omega$ . Spectra remain unchanged over two orders of magnitude in resistance, corresponding to a height change of approximately  $2\ \text{\AA}$ . Dashed line shows fit to Fano line shape, Eq. (10). Curves for  $10R$ ,  $100R$ , and  $1000R$  spectra have been vertically shifted by  $10^{-8}$ ,  $2\times 10^{-8}$ , and  $3\times 10^{-8}$  S, respectively.

bare Au spectra is suppressed in the energy range between  $E_F$  and the surface-state band edge, implying that the cobalt atom “repels” surface-state density over this energy region. In addition, the band-edge feature “A” is replaced by a peak shifted to lower energy (marked “B” in Fig. 1). A new “antiresonance” (marked “C”) also arises near  $E_F$ . Spectra measured over Cu adatoms and herringbone defects both show the shifted band-edge feature marked B, but they show no signs of the narrow resonance near  $E_F$  seen in the cobalt spectrum. These behaviors were observed for numerous cobalt atoms, copper atoms, and herringbone defects at the Au(111) surface. Cobalt atoms located closer than  $10\ \text{\AA}$  from a herringbone domain wall (center to center), however, did show suppression or distortion of feature C.

The cobalt  $E_F$  resonance (feature C) can be seen in greater detail in the higher-resolution spectra of Fig. 2. Here the resonance is observed to display an asymmetric line shape centered slightly above  $E_F$ . Figure 2 shows how this feature varies with vertical distance between the STM tip and a cobalt atom. Each successive spectrum in Fig. 2 was measured after freezing the STM tip at a height corresponding to a factor of 10 increase in the dc tunnel resistance (measured at a bias of  $0.1\ \text{V}$ ). This corresponds to approximately  $1\ \text{\AA}$  in vertical displacement of the STM tip between spectra. The shape of the  $E_F$  resonance varies only slightly with the STM tip height over a vertical range of about  $2\ \text{\AA}$ . At higher tip/surface separation the signal-to-noise ratio is too poor to determine line-shape details. This data shows that while the cobalt  $dI/dV$  spectrum depends strongly on the energy of tunneling electrons, it is not sensitive to local electric-field gradients induced by the tip. It is thus unlikely that the  $E_F$  feature involves field-dependent phenomena, such as the motion of loose adsorbates on the tip or surface.

### C. Surface site and lateral dependence

The line shape of the  $E_F$  resonance, however, does depend on the location of a cobalt atom within the unit cell of

the Au(111) herringbone reconstruction. This dependence was determined by acquiring spectra for atoms naturally adsorbed across the unit cell, as well as for atoms intentionally positioned within it (similar results were obtained in both cases). Atomic manipulation was used to obtain spectra from a single, well-specified cobalt atom positioned at different regions of the surface. Such spectra remove any ambiguity that might exist as to the association of different spectra with a particular type of adsorbate. Figure 3 shows the process of sliding a single cobalt atom to different points within the herringbone unit cell with the aid of the STM tip (sliding impedance= $2\times 10^5\ \Omega$ ). This atom was moved from an fcc region of the reconstruction to a “domain wall,” and then to an hcp region. Figure 4 shows the spectra obtained for this atom in the different regions of the reconstruction. Spectra obtained in the fcc and hcp regions show nearly identical asymmetric line shapes, while the spectrum obtained on the herringbone wall shows strikingly different behavior. The asymmetry of the resonance appears to be reversed when a cobalt atom is positioned at the soliton wall (many Co atoms in this position also showed a complete absence of the  $E_F$  resonance).

The line shape of the  $E_F$  resonance was found to depend on the lateral position of the STM tip with respect to the center of a cobalt atom. This dependence is difficult to quantify, because it varies with the microscopic environment of the cobalt atoms and the detailed structure of the STM tip. In order to systematically study this spatial dependence, spectra were obtained for 10 different cobalt atoms at three different lateral distances from the atoms’ center (all using the same tip). These spectra were then averaged and are plotted in Fig. 5. The averaging here is meant to remove variations due to the location of an atom. At the center position ( $0\ \text{\AA}$ ) the averaged spectra show the familiar asymmetric resonance discussed previously. As the tip of the STM is moved out from the center, however, the line shape becomes more symmetric. This behavior can be seen in the averaged spectra measured at  $4$  and  $11\ \text{\AA}$  from the center of the cobalt atoms.

### D. Coverage dependence

Interactions between cobalt atoms on Au(111) were studied by measuring  $dI/dV$  spectra on cobalt adatoms as a function of cobalt surface density. Figure 6 shows images of the Au(111) surface after successive deposition of cobalt at  $6\ \text{K}$ , resulting in coverages of  $0.02$ ,  $0.05$ ,  $10.1$ , and  $\sim 1$  ML. Figure 7 shows typical spectra measured for individual cobalt atoms at each coverage. The  $E_F$  resonance is clearly seen, and the spectra are all quite similar. The fraction of cobalt atoms showing the  $E_F$  resonance, however, dropped as the coverage was increased. The fraction of atoms showing the resonance in hcp and fcc regions was  $60\%$  for a  $0.025$ -ML coverage,  $54\%$  for a  $0.05$ -ML coverage,  $33\%$  for a  $0.2$ -ML coverage, and only  $14\%$  for the  $\sim 1$ -ML coverage.

## III. DISCUSSION

### A. Overview

In order to interpret these spectroscopic results, we now discuss the electronic structure of transition-metal adsorbates

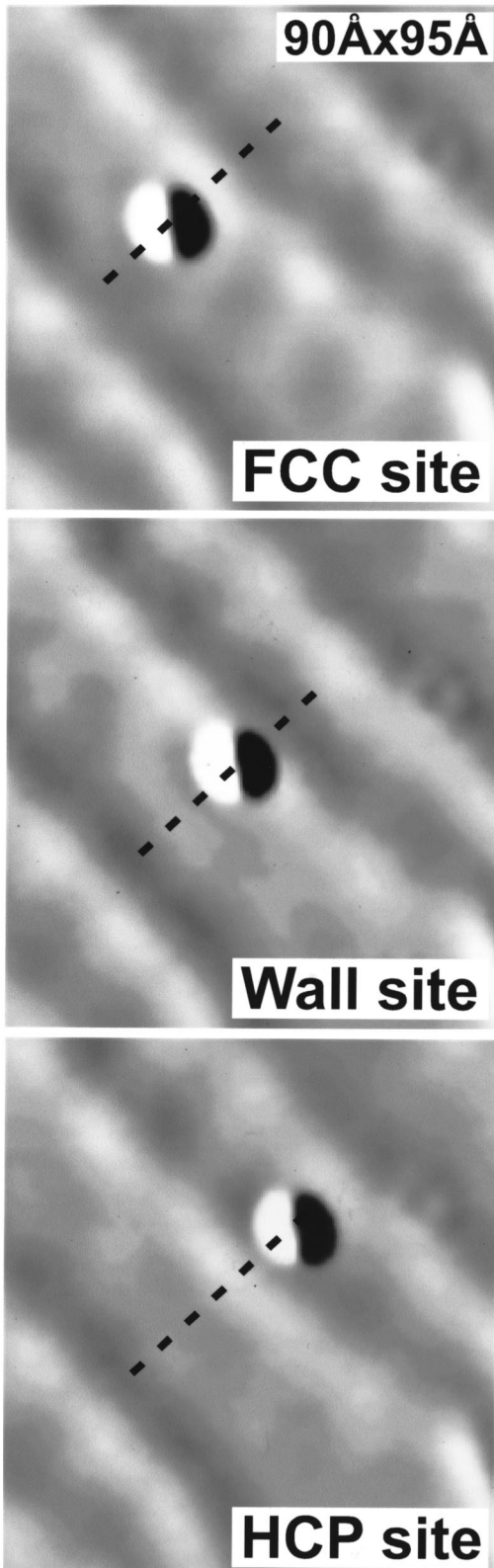


FIG. 3. Three images show the process of using atomic manipulation to move a single Co atom to different sites within the unit cell of the Au(111) herringbone reconstruction. STM spectra acquired for the Co adatom at these different herringbone sites can be seen in Fig. 4. (Derivative images are shown).

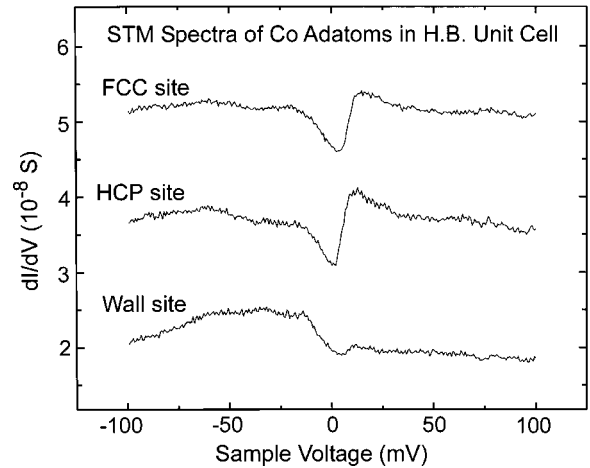


FIG. 4. STM spectra acquired for a single Co adatom positioned on different sites within the Au(111) herringbone unit cell (see images in Fig. 3). The Kondo resonance remains the same for fcc and hcp sites, but the Fano line shape undergoes a sharp change when the adatom is positioned on a soliton wall. fcc-site and wall-site curves have been vertically shifted by  $1.4 \times 10^{-8}$  and  $-1.4 \times 10^{-8}$  S, respectively.

and how this is reflected in tunneling measurements. This topic revolves around the subject of electronic impurity resonances for  $s$ ,  $p$ , and  $d$  orbitals. While an isolated atom has sharp, long-lived energy levels, these levels broaden into resonances when an atom approaches a metal surface.<sup>34,35</sup> Broadening occurs because an electron residing in an adatom orbital can escape into the continuum of substrate electronic states. This topic has been well studied, and the simplest case occurs when the Coulomb interaction between electrons in the adatom orbital is negligible (the “noninteracting” case). Eigenstates of the resonance are then easily calculated within the Anderson/Fano formalism.<sup>18,20</sup> Interpreting experimental measurements of such a resonance, however, is complicated

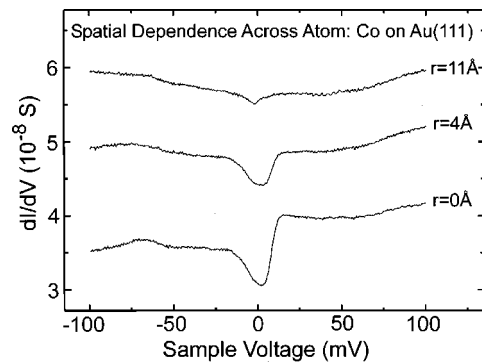


FIG. 5. Distance dependence of the Kondo resonance line shape across individual Co atoms (“ $r$ ” measured from the center of the atom). Average spectra are shown for the STM held at the center of a Co atom ( $0 \text{ \AA}$ ),  $4 \text{ \AA}$  from the center, and  $11 \text{ \AA}$  from the center (each spectrum is averaged over 10 atoms, and all are measured with the same tip). All three spectra have had a linear background slope of  $-2.1 \times 10^{-11} \text{ S/mV}$  removed for viewing. Curves for  $r = 4 \text{ \AA}$  and  $r = 11 \text{ \AA}$  have been vertically shifted by  $0.9 \times 10^{-8}$  and  $1.8 \times 10^{-8}$  S, respectively.

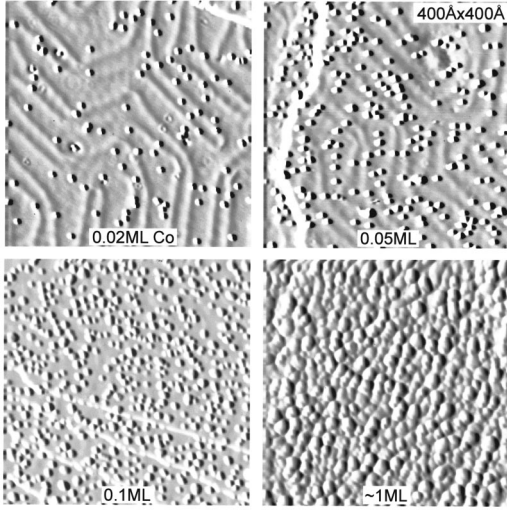


FIG. 6. STM images of the Au(111) surface for different Co coverages of 0.02, 0.05, 0.1, and  $\sim 1$  ML. The crystal was held between 6 and 8 K during deposition and imaging. (Derivative images are shown).

by the relative weighting of the matrix elements coupling the experimental probe to orbital and continuum components of the resonance eigenstates. This problem was first addressed by Fano, whose work explains the well-known spectral line shape of a ‘‘Fano resonance.’’<sup>20</sup>

The electronic behavior of an impurity atom, however, becomes significantly more complex when a strong Coulomb interaction exists between electrons residing in the impurity orbital. This situation leads to a coherent mixing of spin-up and spin-down orbital states, and results in the strongly correlated electronic behavior known as the Kondo effect.<sup>5</sup> In a remarkable simplification, however, it can be shown that spectroscopic measurement near  $E_F$  of a Kondo impurity is equivalent to the measurement of an effective noninteracting impurity state well described within the Fano formalism.<sup>10</sup> Here we will expand on these ideas and apply them toward understanding our local spectroscopic measurements of co-

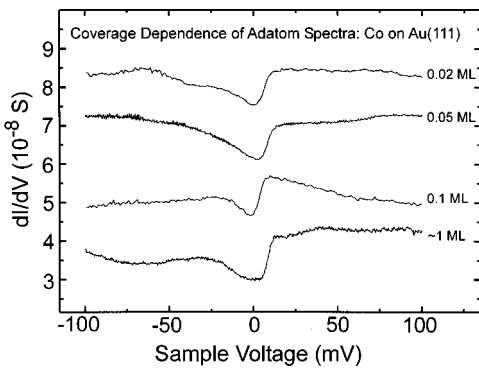


FIG. 7. STM spectra measured over individual Co adatoms at the four different coverages shown in Fig. 6 (0.02, 0.05, 0.1, and  $\sim 1$  ML). The Fano line shape of the Kondo resonance is clearly seen in each case with little variation. Curves for 0.1, 0.05, and 0.02 ML have been vertically shifted by  $1.3 \times 10^{-8}$ ,  $2.8 \times 10^{-8}$ , and  $4.2 \times 10^{-8}$  S, respectively.

balt adsorbates. Our notation has been chosen to correspond as closely as possible to previous theoretical treatments of the Fano resonance.<sup>20,36</sup>

### B. Noninteracting impurity and Fano resonance

We first review the case of noninteracting impurity resonances (i.e., those with no significant Coulomb interactions). This is the situation one might expect when the  $s$  orbital of an adatom hybridizes with a metal surface. A simple description of such a system is the resonant-level model, where an electron is allowed to hop between the discrete atomic orbital and the continuum of electronic band states.<sup>18,20</sup> The Hamiltonian is then

$$\hat{H}_0 = \varepsilon_a a^\dagger a + \sum_k \varepsilon_k c_k^\dagger c_k + \sum_k (V_{ak} a^\dagger c_k + \text{H.c.}). \quad (1)$$

Here  $\varepsilon_a$  is the energy of an electron residing in the discrete atomic state,  $a$  removes an electron from the atomic state,  $c_k$  removes an electron from the  $k$ th band state, and  $V_{ak}$  is the hybridization matrix element connecting the atomic state to the  $k$ th band state. From this Hamiltonian it is straightforward to calculate the advanced atomic-state Green function

$$G_{aa}^0(\varepsilon) = \frac{1}{\varepsilon - [\varepsilon_a + \text{Re} \Sigma_0(\varepsilon) + i \text{Im} \Sigma_0(\varepsilon)]}, \quad (2)$$

where

$$\begin{aligned} \text{Re} \Sigma_0(\varepsilon) &= \sum_k |V_{ak}|^2 \text{P} \left( \frac{1}{\varepsilon - \varepsilon_k} \right), \\ \text{Im} \Sigma_0(\varepsilon) &= \pi \sum_k |V_{ak}|^2 \delta(\varepsilon - \varepsilon_k). \end{aligned} \quad (3)$$

(P denotes Cauchy principal value). The Green function is useful because it leads directly to the atomic-state spectral density  $\rho_a(\varepsilon)$ , an experimentally relevant quantity,

$$\begin{aligned} \rho_a(\varepsilon) &= \frac{1}{\pi} \text{Im} G_{aa}^0(\varepsilon) \\ &= \frac{\text{Im} \Sigma_0(\varepsilon) / \pi}{[\varepsilon - \{\varepsilon_a + \text{Re} \Sigma_0(\varepsilon)\}]^2 + [\text{Im} \Sigma_0(\varepsilon)]^2}. \end{aligned} \quad (4)$$

$\rho_a(\varepsilon)$  describes the local density of states of the atomic state and, assuming  $\Sigma_0(\varepsilon)$  has little energy dependence, is a Lorentzian resonance centered at  $\varepsilon_a + \text{Re} \Sigma_0(\varepsilon)$  with a half-width equal to  $\text{Im} \Sigma_0(\varepsilon)$ .

In a tunneling experiment, a second electrode (the tip) is added to the system and electrons are allowed to tunnel between electrodes. These changes are reflected in the Hamiltonian by adding the terms  $\varepsilon_t t^\dagger t + \hat{M}$  to  $\hat{H}_0$ ,<sup>19</sup>

$$\begin{aligned} \hat{H} &= \varepsilon_a a^\dagger a + \sum_k \varepsilon_k c_k^\dagger c_k + \sum_k (V_{ak} a^\dagger c_k + \text{H.c.}) \\ &\quad + \varepsilon_t t^\dagger t + \hat{M}. \end{aligned} \quad (5)$$

Here the tip is modeled by a single state with energy  $\varepsilon_t$  and  $t$  removes an electron from that state.  $\hat{M}$  is a transfer Hamiltonian term that induces electrons to tunnel from one electrode to the other and is treated as a perturbation.  $\hat{M}$  can be expressed as follows:

$$\hat{M} = (M_{at}a^\dagger t + \text{H.c.}) + \sum_k (M_{kt}c_k^\dagger t + \text{H.c.}) \quad (6)$$

$M_{at}$  and  $M_{kt}$  are the tunnel matrix elements that connect the STM tip to the discrete atomic state and continuum states, respectively.

The STM tunnel current may be expressed as  $I(V) = e\langle \dot{N}_t \rangle$ , where  $N_t = t^\dagger t$ . This expression can be evaluated for the present system and put in a form that closely resembles expressions derived in earlier studies of Fano resonance phenomena<sup>36</sup> (see the Appendix for further details),

$$I(V) = \frac{2e}{\hbar} \int_{-\infty}^{\infty} d\varepsilon \rho_{\text{tip}}(\varepsilon) [f(\varepsilon - eV) - f(\varepsilon)] \cdot \text{Im} \left\{ \sum_k |\hat{M}_{kt}|^2 g_{kk}(\varepsilon) + G_{aa}^0(\varepsilon) [A(\varepsilon) + iB(\varepsilon)] [A^*(\varepsilon) + iB^*(\varepsilon)] \right\}. \quad (7)$$

Here  $\rho_{\text{tip}}$  is the tip density of states and

$$g_{kk}(\varepsilon) = \frac{1}{\varepsilon - \varepsilon_k - i\eta}, \quad \eta \rightarrow 0_+,$$

$$A(\varepsilon) = M_{at} + \sum_k M_{kt} V_{ak} P \left( \frac{1}{\varepsilon - \varepsilon_k} \right), \quad (8)$$

$$B(\varepsilon) = \pi \sum_k M_{kt} V_{ak} \delta(\varepsilon - \varepsilon_k).$$

If we treat  $\rho_{\text{tip}}$  as a constant to reflect the broadening of the tip state by contact with the remainder of the tip electrode, then the low-temperature STM differential conductivity can be found as follows:

$$\frac{dI}{dV}(V) = \frac{2e^2}{\hbar} \rho_{\text{tip}} \cdot \text{Im} \left\{ \sum_k |\hat{M}_{kt}|^2 g_{kk}(eV) + G_{aa}^0(eV) \times [A(eV) + iB(eV)] [A^*(eV) + iB^*(eV)] \right\}. \quad (9)$$

As shown in Ref. 36 and the Appendix, this can be further simplified to the form of a Fano resonance,

$$\frac{dI}{dV}(V) = \frac{2e^2}{\hbar} \rho_{\text{tip}} \left[ \pi \sum_k |\hat{M}_{kt}|^2 \delta(eV - \varepsilon_k) \right] \frac{(\varepsilon' + q)^2}{1 + \varepsilon'^2} + C, \quad (10)$$

where

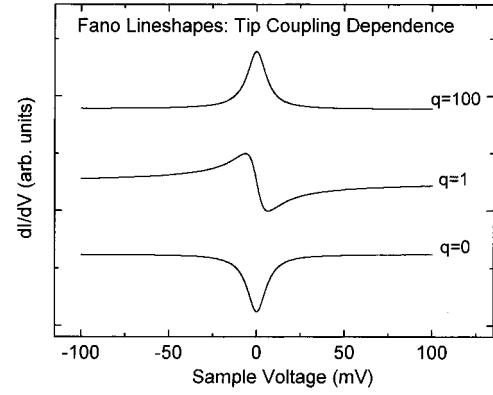


FIG. 8. Theoretical Fano resonance line shape for a resonance at  $E_F$  with half-width = 6.5 mV and a range of different  $q$  parameters [Eq. (10)]. The  $q=100$  case corresponds to strong coupling between the tip and a discrete atomic orbital, and leads to a Lorentzian-like line shape. The  $q=1$  case corresponds to intermediate coupling and leads to an asymmetric resonance. The  $q=0$  case corresponds to the weak-coupling limit and leads to a symmetric dip at  $E_F$  (an antiresonance). (Curves have been vertically shifted for easier viewing).

$$q = \frac{A}{B}, \quad \varepsilon' = \frac{eV - \varepsilon_a - \text{Re} \Sigma_0(eV)}{\text{Im} \Sigma_0(eV)}, \quad (11)$$

and  $C$  is a constant term that depends on conduction-electron states not coupled to the impurity. The atomic-state resonance is thus manifested as a Fano resonance in  $dI/dV$ , the STM differential conductance.

The line shape of the Fano resonance depends on the “coupling parameter”  $q$ . Figure 8 shows a plot of Eq. (10) for three values of  $q$ . If  $q$  is large, the spectrum is Lorentzian, while  $q=1$  leads to an asymmetric spectrum and small  $q$  results in an antiresonance. The physical meaning of  $q$  can be seen in Eqs. (8) and (11). The  $q$  ratio becomes large when either of the two terms in the numerator  $A$  grow relative to the denominator  $B$ . The first term in  $A$  describes direct coupling of the STM tip to the atomic orbital, while the second term in  $A$  describes indirect coupling between the STM tip and the atomic orbital via virtual transitions involving band electrons. The second term in  $A$  is the Hilbert transform of  $B$ , and so reflects any energy dependence that might be present in  $B$  due, for example, to the bandstructure of the substrate. If  $B$  is energy independent then the second term in  $A$  is zero. If  $V_{ak}$  is constant,  $B$  simply gives the coupling of the tip to the unperturbed local density of states LDOS of the metal. In Fano’s original paper,<sup>20</sup> for example, the  $B$  term was physically interpreted as representing coupling between the experimental probe (the STM in our case) and unperturbed continuum LDOS. A large value of  $q$  thus implies that the STM tip is strongly coupled to the atomic orbital (either “directly” or “indirectly”), while a low value of  $q$  implies that the tip is more strongly coupled to the conduction-electron continuum than the atomic orbital. The width of the resonance in either case is  $2 \text{Im} \Sigma_0$ , a factor that depends on the intrinsic coupling between the discrete state and the conduction-electron continuum.

These results can be used to interpret resonance features seen in STM spectra acquired for cobalt adatoms. We first consider feature “*B*” of Fig. 1, an  $87 \pm 7$ -mV-wide resonance centered  $505 \pm 5$  mV below  $E_F$ . The most likely explanation for this resonance is that it is an adsorbate-induced defect state split off from the bottom of the Au(111) surface-state band. This bound state then hybridizes with continuum bulk states. The energy location of the surface state band edge is consistent with this picture, as it lies just  $55 \pm 10$  mV above feature *B*. Such phenomena are well known to occur in other systems.<sup>37,38</sup> An alternative explanation to feature “*B*” is that it directly reflects a cobalt atomic orbital (such as a *d* state). This second explanation is unlikely, however, since feature *B* is observed at the same energy (i.e., just below the surface-state band edge) for cobalt adatoms, copper adatoms, and intrinsic Au-surface defects. The only common feature in all three of these cases is that the Au surface state undergoes a local perturbation. We expect Coulomb interactions to be minimal here since the defect state originates from the gold *sp* band, and so the simple Hamiltonian described in Eq. (1) should be applicable.

The width of feature *B* then comes from the hybridization of the defect state with bulk conduction states (corresponding to  $\text{Im} \Sigma_0$ ). The resonance line shape is nearly Lorentzian, meaning a large value of the *q* parameter. This might be explained by strong coupling between the STM tip and the Au defect state [resulting in a large numerator for *q* in Eq. (11)], as well as by low coupling between the Au defect state and nearby continuum states [resulting in a small denominator for *q* in Eq. (11)]. Such low coupling might be expected between a split-off surface state and nearby orthogonal bulk states below the surface-state band edge.

### C. Interacting impurities and the Kondo resonance

The  $E_F$  resonance seen for cobalt adatoms (feature “*C*” in Fig. 1) has a different physical origin than the band-edge feature just discussed. This is seen first by the fact that the  $E_F$  resonance is located far from the surface-state band edge. Second, the  $E_F$  resonance occurs only for cobalt atoms, whereas the band-edge resonance occurs for cobalt impurities, copper impurities, and intrinsic Au defects. Most important, however, is the fact that the  $E_F$  resonance width is significantly smaller than the width of the band-edge resonance. This is best demonstrated in the high-resolution spectra of Fig. 2. Here the width is only 12 mV when measured from the steep central region of the resonance. This is significantly narrower than the widths expected for *s*-, *p*-, or even *d*-originated adatom resonances. Recent LSDA-based calculations predict a *d*-resonance width of the order of 100 meV for cobalt adatoms on Au(111).<sup>22,39</sup> Careful theoretical treatment of the single-particle excitation spectrum places Co adsorbate *d*-orbital features at least 900 mV from  $E_F$  (measured from the center of the *d* resonance).<sup>22</sup> We believe that the best explanation for the experimentally observed  $E_F$  resonance is that it is the Kondo resonance for a single magnetic impurity.<sup>10</sup> We now discuss how the details of such a resonance can be theoretically understood within the Fano formalism.

Unlike the previous case of a noninteracting resonance, the Kondo effect arises when electrons in an impurity orbital experience strong Coulomb repulsion.<sup>5</sup> This occurs in the *d* orbital of transition-metal impurities. If we consider a single transition-metal impurity having one spin-degenerate *d* orbital, then the Hamiltonian of the system must be modified from Eq. (1) to read

$$\hat{H} = \sum_{\sigma} \varepsilon_d d_{\sigma}^{\dagger} d_{\sigma} + U d_{\sigma}^{\dagger} d_{\sigma} d_{-\sigma}^{\dagger} d_{-\sigma} + \sum_{k,\sigma} \varepsilon_k c_{k\sigma}^{\dagger} c_{k\sigma} + \sum_{k,\sigma} (V_{dk} d_{\sigma}^{\dagger} c_{k\sigma} + \text{H.c.}). \quad (12)$$

Here  $d_{\sigma}$  removes an electron of spin  $\sigma$  from the impurity *d* orbital and  $U$  represents the Coulomb repulsion between two electrons of different spin in a *d* orbital. Only one electron can occupy the *d* orbital at energy  $\varepsilon_d$ , since a second electron, with opposite spin, would have to enter at the increased energy  $\varepsilon_d + U$  (here we ignore *d*-level orbital degeneracy). If  $\varepsilon_d + U > E_F$ , then the spin of the occupied *d* level is unpaired and the impurity is magnetic. Spin-flip processes involving the unpaired spin then lead to a dense set of low-energy excitations that comprise the Kondo resonance and have a half-width of  $k_B T_K$ . The excitation spectrum of a Kondo impurity thus results in three resonances: two “bare” *d* resonances on either side of  $E_F$  at  $\varepsilon_d$  and  $\varepsilon_d + U$ , and the Kondo resonance at  $E_F$ .<sup>5</sup> This physics is reflected in the advanced impurity Green function

$$G_{dd}(\varepsilon) = \frac{1}{\varepsilon - [\varepsilon_d + \text{Re} \Sigma_d(\varepsilon) + i \text{Im} \Sigma_d(\varepsilon)]}. \quad (13)$$

$G_{dd}(\varepsilon)$  has the same general form as the noninteracting expression,  $G_{aa}^0(\varepsilon)$ , but the difference lies in the self-energy term  $\Sigma_d(\varepsilon)$ .  $\Sigma_d(\varepsilon)$  includes the interaction effects not present in  $\Sigma_0(\varepsilon)$  and is in general a complicated function of  $\varepsilon$ . At energies near  $E_F$  and for  $T < T_K$ , however,  $\Sigma_d(\varepsilon)$  can be written in the following simple form:<sup>40</sup>

$$\text{Im} \Sigma_d(\varepsilon) = \frac{\Gamma}{2}, \quad (14)$$

$$\text{Re} \Sigma_d(\varepsilon) = \varepsilon - \varepsilon_d - \frac{(\varepsilon - \alpha)\Gamma}{2k_B T_K},$$

where  $\Gamma$  is the full width of the bare *d* resonance and  $\alpha$  is a constant shift that can arise due to other orbitals, which we have neglected.

In order to understand tunneling measurements into an interacting impurity, one must include the effect of the tip electrode and tunneling processes in the Hamiltonian. Similar to the noninteracting case, this is accomplished by adding  $\Sigma_{\sigma}(\varepsilon, t_{\sigma}^{\dagger} t_{\sigma} + \hat{M}_{\sigma})$  to the Hamiltonian of Eq. (12) (the spin of the tunneling electrons must now be accounted for). The tunnel current can then be calculated identically as for the noninteracting case [Eqs. (7)–(11)], except that  $\Sigma_0(\varepsilon)$  is now replaced by  $\Sigma_d(\varepsilon)$ . This is allowed because the interaction occurs only on the impurity site (see the Appendix for more details). At energies near  $E_F$  and for  $T < T_K$  we can substitute

the expressions for  $\Sigma_d(\varepsilon)$  [Eq. (14)] into Eq. (11) to obtain a narrow Fano resonance having half-width  $k_B T_K$ . The expression for the coupling parameter  $q$  is unchanged from the non-interacting case. The Kondo resonance is thus manifested in  $dI/dV$  as a narrow Fano resonance near  $E_F$ . Despite its origins in the physics of highly correlated electronic phenomena, spectroscopic measurement of the Kondo resonance yields the same result one would expect for a narrow, single-particle resonance near  $E_F$ . This is essentially the same result described in Ref. 10, except that there  $B$  [Eq. (8)] was assumed to be energy independent, an approximation that deemphasizes indirect-coupling contributions to  $q$ . Similar results have also been obtained in other theoretical studies that emphasize indirect tip coupling,<sup>22,23</sup> nonequilibrium effects,<sup>24</sup> and temperature dependence.<sup>21,23</sup>

The Fano resonance expression of Eq. (10) [using the self-energy expressions of Eq. (14)] can be fitted to the cobalt spectra shown in Fig. 2. The spectrum at  $R=2 \times 10^8 \Omega$  yields a Kondo temperature of  $75 \pm 6$  K and a  $q$  value of  $0.60 \pm 0.05$ . The center of the resonance is located at  $6.5 \pm 0.5$  meV above  $E_F$ . No strong variation is seen in these parameters as a function of tip height (i.e., for junction resistances of  $10R$  or  $100R$ ). The value of  $T_K$  found here for cobalt-surface impurities is significantly lower than  $T_K$  values measured for cobalt bulk impurities<sup>25-27</sup> (300–700 K). Such behavior is not unexpected, since the overlap of an impurity  $d$  orbital with conduction states is reduced at a surface compared to the bulk (i.e., from reduced coordination). This tendency is reflected in the approximate expression  $T_K \propto \exp(-1/\rho J)$ , where  $J \propto |V_{dk}|^2 / \min\{|\varepsilon_d|, |\varepsilon_d + U|\}$  and  $\rho$  is the substrate electronic density of states.<sup>5</sup>  $T_K$  is seen to depend exponentially on  $V_{kd}$ , a term that links the impurity  $d$  orbital to conduction states and so is strongly dependent on impurity coordination. Other measurements for Co impurities on a Au surface have been made using a weak localization technique and show an even lower Kondo temperature of  $T_K = 19$  K.<sup>28</sup> One possible explanation for the discrepancy in surface  $T_K$  values is that the weak localization measurements were performed on a disordered gold surface, as opposed to the well-ordered crystal used here.

#### D. Impurity-tip coupling and position dependence:

The fit of Eq. (10) to the cobalt spectrum in Fig. 2 yields information on how the STM tip couples to cobalt impurities via the Fano “ $q$ ” parameter. Because  $q$  is of the order of 1, significant coupling must occur between the STM tip and the cobalt  $d$  orbital. As mentioned in the previous discussion of Eqs. (8) and (11), this coupling can have its origins in two different physical processes: direct coupling (i.e., direct overlap between the tip and the  $d$  orbital) and indirect coupling (i.e., coupling mediated by conduction electrons). In Ref. 10 it was argued that direct coupling dominates, but more recent theoretical studies provide evidence that indirect coupling plays a significant (and even dominant) role.<sup>22,23</sup> Here we argue that indirect coupling to the impurity  $d$  orbital dominates STM tunneling to the Kondo resonance and provides the main contribution to  $q$ . One of the strongest pieces of evidence for this behavior is the lack of tip-height depen-

dence in the spectra of Fig. 2. The electronic decay length of a conduction band state and an impurity  $d$  orbital are expected to be different as one moves away from a surface.<sup>41</sup> If direct coupling played a strong role in the tunneling process, this should result in  $q$  decreasing as the tip is moved vertically away from the impurity atom. Another piece of evidence for the importance of indirect coupling (as pointed out in Ref. 22) comes from the recent “quantum mirage” work of Manoharan, Lutz, and Eigler. In that work a Kondo/Fano resonance with nonzero  $q$  is observed at the empty focus of an ellipsoidal quantum corral, opposite a focus containing a Kondo impurity. There is no possibility of a direct-coupling term at the empty focus, yet  $q$  remains nonzero for spectra taken at that point (and so must be entirely due to indirect coupling). Dominance of the indirect-coupling term over the direct-coupling term is not surprising, due to the tightly bound nature of the  $d$  orbital, which minimizes direct tip overlap. The indirect contribution to  $q$  can be calculated from the terms in Eq. (8) if the electronic structure of the substrate is known. Some initial calculations have been performed that extract values of  $q$  from a model electronic structure.<sup>22</sup>

The coupling between the STM tip and the impurity  $d$  orbital varies dramatically with the impurity position on the reconstructed Au(111) surface. Fits made to the spectra displayed in Fig. 4 show that the  $q$  factor changes from  $+0.68 \pm 0.02$  to  $-1.5 \pm 0.3$  when a cobalt atom is moved from an fcc region to a reconstruction domain wall ( $T_K$  is also slightly raised). These changes in  $q$  most likely come about from variations in the local electronic structure induced by the herringbone reconstruction. Such variation arises from the influence of the reconstruction potential on two-dimensional surface-state electrons, and has been observed in previous studies.<sup>32,33</sup> Variations in the tip-coupling parameter are somewhat less dramatic when the STM tip is moved laterally across the surface of an individual cobalt atom. Fits to the spectra in Fig. 5 show the average value of  $q$  changing from  $+0.58 \pm 0.02$  when the tip is held over the center of a cobalt atom to  $+0.30 \pm 0.01$  when the tip is shifted 4 Å off center. This reduction in  $q$  points to a lessening of the coupling between the tip and the impurity  $d$  orbital as the tip is moved off center. Such dependence arises from spatial variation in the matrix element  $M_{tk}$ , as well as substrate bandstructure.

#### E. Cobalt density dependence and interactions

It is striking that the cobalt-surface concentration does not have a large impact on the Fano resonance line shape. The overall percentage of atoms showing the Kondo resonance does decrease with coverage, but those atoms displaying the resonance in the hcp and fcc regions of the reconstruction show no strong concentration dependence in their spectral line shape. The lower percentage of atoms showing the Kondo resonance at increased coverage might be explained by clustering of atoms. As the cobalt coverage increases, single-atom-like structures on the surface have a higher probability of actually incorporating multiple impurities. It is known from previous work that cobalt dimers, for example, do not show Kondo resonance.<sup>17</sup> For atoms showing a

Kondo resonance, the lack of strong concentration dependence has two implications. First, it implies that impurity-induced surface-state interference effects do not play a significant role in cobalt Kondo impurity behavior on gold. While one does expect the Au(111) surface state to be perturbed as the density of surface scatterers is increased, the lack of any significant influence on the Kondo resonance implies that cobalt impurities are not strongly affected by these changes. Second, this behavior implies that indirect magnetic coupling (“RKKY” coupling<sup>6</sup>) between cobalt atoms is not significant at the surface of gold. One expects that strong RKKY coupling between cobalt atoms would lead to spin-glass behavior and modifications to the Kondo effect from impurity-impurity spin interactions.<sup>42–44</sup> The lack of any significant density dependence in Kondo behavior for our data implies that the RKKY coupling energy is smaller than the Kondo binding energy ( $k_B T_K$ ). This behavior is consistent with a previous experimental study of cobalt dimers,<sup>17</sup> as well as theoretical studies of the short-range character of impurity spin-spin interactions.<sup>45</sup>

#### IV. SUMMARY

In conclusion, we have used a cryogenic UHV STM to investigate the local electronic structure of cobalt atoms adsorbed to Au(111). We find two distinct resonances, one near  $E_F$  and the other just below the surface-state band edge. The band-edge resonance is believed to be a Au defect state, but the  $E_F$  resonance is believed to be a many-body Kondo resonance. The Kondo resonance does not change significantly with tip height above the cobalt atom, but it does vary with atom placement on the Au(111) surface and with lateral tip position relative to the impurity center. The surface concentration of cobalt atoms is observed to have little effect on the details of the Kondo resonance. We show theoretically that impurity resonances observed via STM spectroscopy are, in general, a class of Fano resonance. This is true for noninteracting resonances (i.e., impurity orbitals with negligible Coulomb interactions) as well as for strongly interacting impurity resonances (i.e., orbitals with significant Coulomb interactions). Using the Anderson model we show that tunneling into a strongly interacting impurity  $d$  orbital should lead to a narrow Fano resonance near  $E_F$ , which is a reflection of the Kondo resonance. As with the case of noninteracting impurities, the line shape of the Kondo/Fano resonance depends on the degree of coupling between the STM tip and the impurity  $d$  orbital. This coupling can be either direct or indirect, but it is argued that indirect coupling dominates for cobalt on Au(111). This explains the lack of tip-height dependence of the cobalt spectra and, together with the surface electronic structure, forms a framework to explain the spectral dependence on impurity-surface location and lateral tip position. The cobalt concentration dependence of the Kondo resonance implies atomic clustering at high coverage and weak RKKY coupling between cobalt impurities.

#### ACKNOWLEDGMENTS

M.F.C. wishes to acknowledge useful discussions with H. Kroha, A. Zawadowski, A. Schiller, and V. Stepanyuk. This

work was supported in part by NSF DMR-9971690 and by the Director, Office of Energy Research, Office of Basic Energy Science Division of the U.S. Department of Energy under Contract No. DE-AC03-76SF0098.

#### APPENDIX

Here we derive Eqs. (7)–(11) for the more general case of an interacting impurity ( $U \neq 0$ ), as represented by the Hamiltonian of Eq. (12). To explicitly reproduce Eqs. (7)–(11), substitute  $a$  for  $d$ , let  $U=0$ , and remove the sum over spins. We begin with  $I(V) = e \langle \dot{N}_t \rangle$ , where  $N_t = \sum_{\sigma} t_{\sigma}^{\dagger} t_{\sigma}$ . This can be reexpressed in the following manner:

$$\begin{aligned} I &= e \langle \dot{N}_t \rangle = \frac{ie}{\hbar} \langle [H, N_t] \rangle \\ &= -\frac{ie}{\hbar} \left[ \sum_{k\sigma} (M_{kt} \langle c_{k\sigma}^{\dagger} t \rangle - \text{H.c.}) \right. \\ &\quad \left. + \sum_{\sigma} (M_{dt} \langle d_{\sigma}^{\dagger} t \rangle - \text{H.c.}) \right], \end{aligned}$$

$\langle c_{k\sigma}^{\dagger} t \rangle$  and  $\langle d_{\sigma}^{\dagger} t \rangle$  can be expanded to leading order in  $M$  to calculate STM tunnel current using Fermi’s Golden rule. This gives

$$\begin{aligned} I &= -\frac{2ie}{\hbar} \int_{-\infty}^{\infty} d\varepsilon \rho_{\text{tip}}(\varepsilon) [f(\varepsilon - eV) - f(\varepsilon)] \\ &\quad \times \left\{ \sum_{kk'} M_{kt} M_{k't}^* (G_{k't}^a - G_{k't}^r) + \sum_k M_{kt} M_{dt}^* (G_{dk}^a - G_{dk}^r) \right. \\ &\quad \left. + \sum_k M_{kt}^* M_{dt} (G_{kd}^a - G_{kd}^r) + |M_{dt}|^2 (G_{dd}^a - G_{dd}^r) \right\}. \end{aligned}$$

Here  $G_{dd}^{r/a}$  and  $G_{dk}^{r/a}$  are the full advanced and retarded Green functions between band states (the continuum) and  $d$  orbitals (discrete states) in the absence of coupling to the STM tip.

Because interactions occur only for electrons in  $d$  orbitals, the Green functions involving band states can be factored,

$$G_{dk}^{r/a} = V_{dk} G_{dd}^{r/a} g_{kk}^{r/a},$$

$$G_{k't}^{r/a} = g_{kk}^{r/a} \delta_{kk'} + V_{dk} V_{dk'}^* g_{k'k}^{r/a} G_{dd}^{r/a} g_{kk}^{r/a}.$$

Here  $g_{kk}^{r/a}$  are Green functions of band states unperturbed by the impurity, so all interactions are contained in  $G_{dd}^{r/a}$  (with an extra factor of 2 for spin). This leads to the conductance expression of Eq. (7)

$$\begin{aligned} I &= \frac{4e}{\hbar} \int_{-\infty}^{\infty} d\varepsilon \rho_{\text{tip}}(\varepsilon) [f(\varepsilon - eV) - f(\varepsilon)] \\ &\quad \times \text{Im} \left\{ \sum_k |M_{kt}|^2 g_{kk}^a(\varepsilon) + G_{dd}^a(\varepsilon) [A(\varepsilon) + iB(\varepsilon)] \right. \\ &\quad \left. \times [A^*(\varepsilon) + iB^*(\varepsilon)] \right\}, \end{aligned}$$

where

$$A(\varepsilon) = M_{dt} + \sum_k M_{kt} V_{dk} P\left(\frac{1}{\varepsilon - \varepsilon_k}\right) \quad \text{and}$$

$$B(\varepsilon) = \pi \sum_k M_{kt} V_{dk} \delta(\varepsilon - \varepsilon_k).$$

To get a Fano-like form for  $dI/dV$ , note that

$$G_{dd}^a(\varepsilon) = \frac{1}{\varepsilon - [\varepsilon_d + \text{Re} \Sigma_d(\varepsilon) + i \text{Im} \Sigma_d(\varepsilon)]}$$

and define

$$\varepsilon' = \frac{eV - \varepsilon_d - \text{Re} \Sigma_d(eV)}{\text{Im} \Sigma_d(eV)},$$

$$qe^{i\theta} = \frac{A}{B}.$$

This gives

$$\frac{dI}{dV} = \frac{4e^2}{\hbar} \rho_{\text{tip}} \left\{ \pi \sum_k |M_{kt}|^2 \delta(eV - \varepsilon_k) + \frac{|B|^2}{\text{Im} \Sigma_d(eV)} \frac{q^2 - 1 + 2q\varepsilon' \cos \theta}{1 + \varepsilon'^2} \right\}.$$

If no magnetic field is present,  $A$  and  $B$  are real, so  $\cos \theta = 1$ . The sum in the first term of the expression for  $dI/dV$  can be separated into  $k$  states that couple to the impurity and  $k$  states that do not couple to the impurity. The latter form a constant background. For a single-band model the contribution from  $k$  states that couple to the impurity is exactly

$$\frac{|B|^2}{\text{Im} \Sigma_d(eV)}.$$

This results in the classic Fano expression, Eq. (10) (but with an added factor of 2 for spin),

$$\frac{dI}{dV}(V) = \frac{4e^2}{\hbar} \rho_{\text{tip}} \left[ \pi \sum_k |\hat{M}_{tk}|^2 \delta(eV - \varepsilon_k) \right] \frac{(\varepsilon' + q)^2}{1 + \varepsilon'^2} + C.$$

\*Present address: Condensed Matter Physics, Caltech 114-36, Pasadena, CA 91125.

<sup>1</sup>I. K. Schuller, S. Kim, and C. Leighton, *J. Magn. Magn. Mater.* **200**, 571 (1999).

<sup>2</sup>A. P. Ramirez, *J. Phys.: Condens. Matter* **9**, 8171 (1997).

<sup>3</sup>J. S. Moodera and G. Mathon, *J. Magn. Magn. Mater.* **200**, 248 (1999).

<sup>4</sup>S. Heinze, M. Rode, A. Kubetzka, O. Pietzsch, X. Nie, S. Blugel, and R. Wiesendanger, *Science* **288**, 1805 (2000).

<sup>5</sup>A. C. Hewson, *The Kondo Problem to Heavy Fermions* (Cambridge University Press, Cambridge, 1993).

<sup>6</sup>R. M. White, *Quantum Theory of Magnetism* (Springer-Verlag, New York, 1983).

<sup>7</sup>E. L. Wolf, *Principles of Electron Tunneling Microscopy* (Oxford University Press, New York, 1985).

<sup>8</sup>S. Gregory, *Phys. Rev. Lett.* **68**, 2070 (1992).

<sup>9</sup>D. C. Ralph and R. A. Buhrman, *Phys. Rev. Lett.* **72**, 3401 (1994).

<sup>10</sup>V. Madhavan, W. Chen, T. Jamneala, M. F. Crommie, and N. S. Wingreen, *Science* **280**, 567 (1998).

<sup>11</sup>J. Li, W.-D. Schneider, R. Berndt, and B. Delley, *Phys. Rev. Lett.* **80**, 2893 (1998).

<sup>12</sup>H. C. Manoharan, C. P. Lutz, and D. M. Eigler, *Nature (London)* **403**, 512 (2000).

<sup>13</sup>T. Jamneala, V. Madhavan, W. Chen, and M. F. Crommie, *Phys. Rev. B* **61**, 9990 (2000).

<sup>14</sup>M. F. Crommie, C. P. Lutz, and D. M. Eigler, *Phys. Rev. B* **48**, 2851 (1993).

<sup>15</sup>R. Wiesendanger, M. Bode, M. Kleiber, M. Loehndorf, R. Pascal, A. Wadas, and D. Weiss, *J. Vac. Sci. Technol. B* **15**, 1330 (1997).

<sup>16</sup>A. Yazdani, B. A. Jones, C. P. Lutz, M. F. Crommie, and D. M. Eigler, *Science* **275**, 1767 (1997).

<sup>17</sup>W. Chen, T. Jamneala, V. Madhavan, and M. F. Crommie, *Phys. Rev. B* **60**, R8529 (1999).

<sup>18</sup>P. W. Anderson, *Phys. Rev.* **124**, 41 (1961).

<sup>19</sup>G. D. Mahan, *Many-Particle Physics* (Plenum, New York, 1990).

<sup>20</sup>U. Fano, *Phys. Rev.* **124**, 1866 (1961).

<sup>21</sup>T. Kawasaki, H. Kasai, W. A. Dino, and A. Okiji, *J. Appl. Phys.* **86**, 6970 (1999).

<sup>22</sup>O. Ujsaghy, J. Kroha, L. Szunyogh, and A. Zawadowski, *Phys. Rev. Lett.* **85**, 2557 (2000).

<sup>23</sup>A. Schiller and S. Hershfield, *Phys. Rev. B* **61**, 9036 (2000).

<sup>24</sup>M. Plihal and J. W. Gadzuk, *Phys. Rev. B* **63**, 085404 (2001).

<sup>25</sup>G. Gruener and A. Zawadowski, *Rep. Prog. Phys.* **37**, 1497 (1974).

<sup>26</sup>D. Riegel and K. D. Gross, *Physica B* **163**, 678 (1990).

<sup>27</sup>M. D. Daybell and W. A. Steyert, *Rev. Mod. Phys.* **40**, 380 (1968).

<sup>28</sup>W. Wei, R. Rosenbaum, and G. Bergmann, *Phys. Rev. B* **39**, 4568 (1989).

<sup>29</sup>C. Woll, S. Chiang, R. J. Wilson, and P. H. Lippel, *Phys. Rev. B* **39**, 7988 (1988).

<sup>30</sup>S. D. Kevan and R. H. Gaylord, *Phys. Rev. B* **36**, 5809 (1987).

<sup>31</sup>N. D. Lang, *Phys. Rev. B* **34**, 5947 (1986).

<sup>32</sup>D. Fujita, K. Amemiya, T. Yakabe, H. Nejoh, T. Sato, and M. Iwatsuki, *Phys. Rev. Lett.* **78**, 3904 (1997).

<sup>33</sup>W. Chen, V. Madhavan, T. Jamneala, and M. F. Crommie, *Phys. Rev. Lett.* **80**, 1469 (1998).

<sup>34</sup>J. W. Gadzuk, *Phys. Rev. B* **1**, 2110 (1970).

<sup>35</sup>E. W. Plummer and R. D. Young, *Phys. Rev. B* **1**, 2088 (1970).

<sup>36</sup>A. Shibatani and Y. Toyozawa, *J. Phys. Soc. Jpn.* **25**, 335 (1968).

<sup>37</sup>A. Zangwill, *Physics at Surfaces* (Cambridge University Press, Cambridge, 1988).

<sup>38</sup>S. G. Davison and M. Steslicka, *Basic Theory of Surface States* (Clarendon Oxford, 1992).

- <sup>39</sup>M. Weissmann, A. Saul, A. M. Llois, and J. Guevara, *Phys. Rev. B* **59**, 8405 (1999).
- <sup>40</sup>A. Houghton, N. Read, and H. Won, *Phys. Rev. B* **35**, 5123 (1987).
- <sup>41</sup>N. D. Lang, *Phys. Rev. Lett.* **56**, 1164 (1986).
- <sup>42</sup>E. Boucai, B. Lecoanet, J. Pilon, J. L. Tholence, and R. Tournier, *Phys. Rev. B* **3**, 3834 (1971).
- <sup>43</sup>G. Gruener and E. Babic, *Physica B & C* **86–88**, 850 (1977).
- <sup>44</sup>A. W. Sheikh, *J. Phys. F: Met. Phys.* **18**, 2015 (1988).
- <sup>45</sup>V. Barzykin and I. Affleck, *Phys. Rev. B* **61**, 6170 (2000).